Hindawi
Journal of Mathematics
Volume 2022, Article ID 1464695, 14 pages
https://doi.org/10.1155/2022/1464695

Research Article

Similarity and Finite Difference Solution on Biomagnetic Flow and Heat Transfer of Blood-Fe_3O_4 through a Thin Needle

Abdulaziz Alsenafi [1] **and M. Ferdows** [2]

[1]*Department of Mathematics, Kuwait University, Safat, Kuwait*
[2]*Department of Applied Mathematics, University of Dhaka, Dhaka, Bangladesh*

Correspondence should be addressed to Abdulaziz Alsenafi; abdulaziz.alsenafi@ku.edu.kw

Received 13 August 2022; Revised 7 November 2022; Accepted 10 December 2022; Published 22 December 2022

Academic Editor: Serkan Araci

A magnetic fluid is composed of a base fluid and magnetic particles, where magnetic particles are carefully distraught in the base fluid. Here, we will assume that blood is the base fluid that exhibits electrical conductivity and polarization properties and Fe_3O_4 as magnetic particles. The addition of Fe_3O_4 into the blood can remarkably ameliorate the properties of the blood's thermal conductivity. Such physical aspects can play a vital role in biomedical and bioengineering. The presented model studies the biomagnetic fluid flow, such as blood that contains magnetic particles through a thin needle in the appearance of a strong magnetic dipole. First, the governing equations are transformed using similarity transformation into a system of dimensional differential equations, which are then nondimensionalized. The system of nondimensional equations is then solved numerically using a finite difference method. By analyzing the results, we find that the axial flow decreases for the ferromagnetic number, magnetic field number, and Eckert number, while the temperature increases with volume fraction, where the size of the needle plays a significant role. Finally, the results also indicate that the presence of ferromagnetism significantly influences the skin friction coefficient. Our presented results will also be compared with existing literature that is similar to our work.

1. Introduction

In fluid dynamics, the study of mechanical properties of biological fluid in the presence of a strong applied magnetic field is commonly known as biomagnetic fluid dynamics (BFDs). Recently, BFDs have been extensively researched due to their versatile applications in the fields of medicine and bioengineering. Moreover, examples of such applications are included but are not limited to magnetic drug targeting [1], magnetic cell separation [2], reducing the flow of blood during surgeries [3], cancer tumor treatment [4], cell death by hypothermia [5], and magnetic resonance imaging (MRI) [6]. Furthermore, this type of fluid, such as blood, can also exist in our human body; blood possesses electrical conductivity and magnetization properties due to the existence of ions in the plasma. Therefore, to investigate the plenary properties of blood, which include magnetization along with electrical conductivity, a new extended mathematical model of BFD was developed.

Magnetic fluid is a new class of fluids in which magnetic particles such as Fe_3O_4 and Co-Fe_2O_4 are suspended in a base fluid such as blood. These magnetic fluids (blood-Fe_3O_4) are usually used to enrich and decrease the thermal conductivity of materials by introducing metallic elements, where the dimensions of particles considered are between 1 and 100 nm. Moreover, the fluids can help improve the performance of blood-Fe_3O_4 flow and the heat transfer rate. This has further motivated us to investigate the mechanism of blood-Fe_3O_4 flow subject to a strong magnetic field within various conditions through a thin cylindrical needle surface. The suspension of particles modifies the transport properties of the base fluids. A theoretical investigation on nanofluid was performed in the study of Choi and Eastman [7], where the authors show that the thermal conductivity properties are enriched when nanoparticles are added to the base fluid.

Due to the importance of nanofluid, various researches were performed by different authors, which include Nadeem et al. [8], Nayak [9], and Khan and Pop [10]. The impacts of a magnetic field on the blood flow through a cylindrical tube with magnetic particles are examined by Ali et al. [11]. In their work, Ali et al. found that the MHD parameter's motion of nanofluid slightly decreases, which could be effective in drug delivery and controlling blood flow.

Alam et al. [12] presented an extended mathematical model of BFD through a two-dimensional stretching cylinder. Their mathematical model was constructed with FHD and MHD principles, in which the authors considered blood as their base fluid and Fe_3O_4 as magnetic particles. Ferdows et al. [13] investigated the behavior of normal blood flow over a stretching cylinder under the mutual interactions of FHD and MHD. In their investigation, the authors showed that the lowest velocity of blood is attained for BFD formulation. In contrast, the highest temperature is reached for BFD formulation compared to MHD and FHD formulations. A similar investigation was also performed by Alam et al. [14]. In [15], Sharma et al. performed an MHD mathematical model to simulate the flow of blood and magnetic particles in a cylindrical tube and found that the velocity of blood and magnetic particles significantly changes in the presence of a magnetic field. Finally, by approaching the Caputo-Fabrizio derivation, Ali et al. [16] examined a non-Newtonian blood flow model along with magnetic particles under the influence of a magnetic field.

Due to the biomedicine applications of thin needles, such as cancer therapy and dermic administration of drugs, research on blood flow models associated with thin needles has increased. Geometrically, a tenor body that is revolved parabolically is known as a thin needle in which the external flow through the thin needle is axisymmetric. Hayat et al. [17] studied the stagnation point of the boundary layer flow of water-carbon with variable surface heat flux in a horizontal needle. Salleh et al. [18] studied both the flow and heat transfer of magnetohydrodynamics nanofluid through a moving thin. Furthermore, the heat transfer of water-based radiative nanofluid flow with entropy generation through a moving thin needle was studied by Waleed Ahmed Khan et al. [19]. In [20], Aladdin et al. examined a two-dimensional boundary layer mathematical model of heat and flow of Cu-Al_2O_3/water by a thin needle. Their resulting system of equations was solved numerically by using Matlab's bvp4c function. Finally, the magnetohydrodynamic mixed convection flow of ceramics nanofluid with variable fluid properties due to a thin needle is perused by Nayak et al. [21].

A stream analysis using the Koo and Kleinstreuer model for two different alloys such as AA7075 and AA7072 in a water-based nanofluid flow over a two-dimensional stretching sheet under the influence of magnetic dipole is studied by Ganesh Kumar [22]. Furthermore, in [23], Reddy et al. studied dynamic and static approaches for aluminum alloys such as AA7075 over a semi-infinite plate that was heated in a Darcy–Forchheimer porous media. In [24], the authors investigated the dual behavior of Fe_2O_4-Cu water hybrid nanofluid over a moving plate in the presence of thermal radiation. They found that the heat transfer of fluid enhanced under the presence of thermal radiation, while a reduction of heat transfer is seen for the Prandtl number.

In [25], Souyaeh et al. discussed the flow and heat transfer of Fe_2So_4-TiAl4V water hybrid nanofluid along with the suspension of dusty fluid over a 2D stretching sheet under the effects of both thermal radiation and slip effects. They saw that the heat transmission process is more effective in hybrid nanofluid cases compared to that of a nanofluid model. Furthermore, in [26], the authors performed a least square approach to study the effects of spherically shaped particles on the Fe_2O_3-Se water hybrid nanofluid under a moving frame using the Rosseland approximation. Reddy et al. [27] analyzed the hydrodynamic flow of dusty fluid over a stretching sheet with the aid of slip effects. They found that the skin friction coefficient attained its highest for a single-wall carbon nanotube compared to those of multiple carbon nanotubes. Additionally, a Cattaneo–Christov heat flux model that studies a hybrid dusty fluid flow was performed in [28]. Additionally, the Cattaneo–Christov heat flux model was also used in [29], but this time it was performed on carbon nanotubes that were filled with liquid over a melting surface.

In [30], Das et al. constructed a mathematical model in order to analyze the dynamism of the blood flow stream with Ag-Al_2O_3 nanoparticles in a nonuniform endoscopic conduit with accounting joule heating and heat source effects. Furthermore, Das et al. [31] discussed the flow characteristics of blood containing copper and gold nanoparticles over a nonuniform endoscopic annulus along a slip wall under the influence of hall currents and electromagnetic force. They found that the temperature of blood drops whenever the volume fraction increases. In [32], the authors studied the electromagnetism of a hybrid nanoblood that was pumped via an endoscope in the presence of hall and ion slip currents. The impacts of the hall currents, electromagnetic force, and heat source on blood-based hybrid-nanofluid flow where copper and copper oxide were considered as nanoparticles through an inclined artery having mild stenosis are also studied in [33]. The authors found that the hemodynamic resistance would increase approximately two times whenever 0.11% nanoparticles are suspended in the blood flow. The authors also noticed that the blood temperature slows down considerably whenever the Cu-CuO nanoparticles were injected, compared to that of pure blood and Cu-blood. In [34], Das et al. provided a theoretical study about the blood flow through an endoscope with peristaltic waves under the influence of hall and ion slip currents. Additionally, in [35], Ali et al. studied the significance of entropy generation for peristaltic blood flow through a tube conveying nanoparticles.

In [36], Alwawi et al. studied the MHD free convection sodium alginate flow with TiO_2, Ag, and GO nanoparticles through a solid sphere with a prescribed wall temperature. Swalmeh et al. [37] presented numerical solutions with natural convection boundary layer flow of Cu and Al_2O_3 water-based nanofluid on a solid sphere using the Keller-box method. In [38], the authors examined the kerosene oil (as Casson fluid) flow over a circular cylinder under an MHD

effect. Hamarsheh et al. [39] investigated the natural convection of Casson fluid (methanol as host fluid) flow in a horizontal cylinder under the impact of a magnetic force and volume fraction.

A comprehensive study about the flow of blood while considering both the Newtonian and non-Newtonian characteristics in arteries is provided by Thomas and Sumam [40], in which they found that the non-Newtonian behavior of blood in small arteries will give more relevancy. A complete understanding of blood flow of the relationship between pressure, viscosity, and symptoms of cardiovascular stenoses is provided by Ku [41]. Other studies of blood flow in larger arteries along with rheology, viscosity models, and physiologic conditions are available in the study by Yilmaz and Gundogdu [42]. This review unifies the entirety of the available information regarding the restrictions on experimental results obtained using a rheometer, more recent hemorheological models, and pertinent data.

The novelty of our present work is to investigate the effect of electrical conductivity and polarization on biomagnetic fluid (blood) containing Fe_3O_4 magnetic particles over a thin needle. The impacts of the MHD parameter, FHD parameter, and the volume fraction of magnetic particles are taken into consideration. Our considered model will monitor fluid motion over a two-dimensional thin needle. The proposed mathematical model is solved by utilizing similarity transformations so that our PDEs are transformed into a system of ODEs, which are then nondimensionalized. The dimensionless ODE system is then numerically solved using a finite difference method with a central difference scheme. We will both mathematically and physically analyze the results by relating them to the original physical problem. Moreover, our results will look at a parametric study where the axial velocity, temperature distributions, skin friction coefficient, and heat transfer rate are all examined. Finally, to validate our results, we will compare the results obtained through our simulations with earlier published work. We hope our results could be used in different applications such as in the medical field for drug administration and cancer treatment.

2. Formulation of the Problem

We consider a steady incompressible laminar flow of biomagnetic fluid. The fluid is assumed to be electrically conducting with magnetic particles around a thin heated needle, as shown in Figure 1. Additionally, we also consider the following assumptions:

(i) The magnetic fluid is appurtenant of a base fluid that is blood with magnetic particles Fe_3O_4

(ii) Thermal equilibrium is fulfilled between the blood and Fe_3O_4

(iii) The needle moves horizontally with velocity $U = u_w + u_\infty$, where u_w and u_∞ represent the velocity of the needle and ambient fluid, respectively

(iv) The size of the needle is denoted by c, whereas the radius of the needle is $r = R = (\nu_f cx/U)^{1/2}$, where x and r represent the axial and radial directions, respectively

(v) The temperature of the sheet and ambient fluid temperature is T_w and T_c, respectively, with $T_w < T_c$

(vi) A magnetic dipole generates a strong magnetic field of intensity H that is kept the distance d from the cylindrical surface

(vii) The physical effect of radiative heat flux has sufficiently small in the direction parallel to the surface such that it can be neglected

Our work is motivated by that references [12, 43–46]. By considering our assumptions and following the aforementioned references, the corresponding continuity, momentum, and energy equations in the cylindrical coordinates take the following form:

$$\frac{\partial}{\partial x}(ru) + \frac{\partial}{\partial r}(rv) = 0, \tag{1}$$

$$u\frac{\partial u}{\partial x} + v\frac{\partial u}{\partial r} = \frac{\mu_{mf}}{\rho_{mf}}\left(\frac{1}{r}\frac{\partial u}{\partial r} + \frac{\partial^2 u}{\partial r^2}\right) - \frac{\sigma_{mf}}{\rho_{mf}}B^2 u + \frac{\mu_0}{\rho_{mf}}M\frac{\partial H}{\partial x}, \tag{2}$$

$$\left(\rho C_p\right)_{mf}\left(u\frac{\partial T}{\partial x} + v\frac{\partial T}{\partial r}\right) + \mu_0 T\frac{\partial M}{\partial T}\left(u\frac{\partial H}{\partial x} + v\frac{\partial H}{\partial r}\right) = \kappa_{mf}\left[\frac{1}{r}\frac{\partial}{\partial r}\left(r\frac{\partial T}{\partial r}\right)\right] + \frac{\sigma_{mf}}{\rho_{mf}}B^2 u^2. \tag{3}$$

With the boundary conditions following that of references [44, 45]:

When $r = R$, we have that

$$\begin{aligned} u &= u_w, \\ v &= 0, \\ T &= T_w. \end{aligned} \tag{4}$$

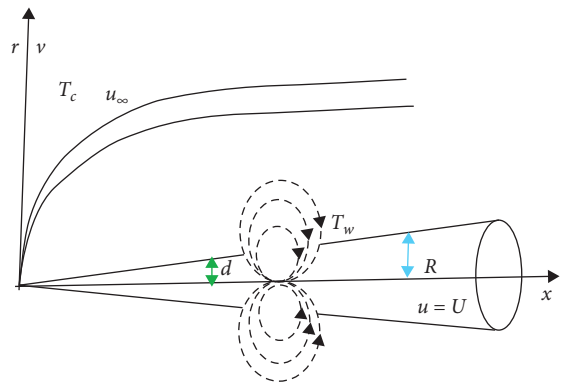

Figure 1: Geometry flow model of the problem along with the coordinate system [43].

and when $r \longrightarrow \infty$, we have that

$$u \longrightarrow u_\infty, T \longrightarrow T_c. \tag{5}$$

The velocity components (u, v) represent the axial x and the radial r direction, respectively. Additionally, the parameters $\rho, C_p, \kappa, \mu, \mu_0$, and σ represent the blood (as biomagnetic fluid) density, specific heat, thermal conductivity, dynamic viscosity, magnetic permeability, and electrical conductivity, respectively. The magnetic field of strength is mathematically denoted by $H = (H_x, H_r)$, and $B = \mu_0 H$ represents the magnetic induction. The subscript symbol $_{mf}$ represents the magnetic fluid, which is the base fluid (as blood) mixed with magnetic particles (as Fe_3O_4).

From [47, 48], we know that the term Lorentz force arises because of the term $-(\sigma_{mf}/\rho_{mf})B^2u$, which is included in (2), whereas the term $(\sigma_{mf}/\rho_{mf})B^2u^2$ on the right-hand side of (3) represents the Joule heating. Both terms emerge due to the electrical conductivity of blood. Now, due to the presence of the magnetic gradient, as we see in the study of FHD in [49–51], the magnetic force per unit volume along the axial x direction is caused by $(\mu_0/\rho_{mf})M(\partial H/\partial x)$, whereas the term $\mu_0 T(\partial M/\partial T)(u(\partial H/\partial x) + v(\partial H/\partial r))$ accounts for the heating that is owned to adiabatic magnetization.

As cited in [49–51], the magnetic dipole raises the magnetic field by saturating the bio-fluid sufficiently and is written as follows:

$$V = \frac{\delta}{2\pi} \cdot \frac{x}{x^2 + (r+d)^2}, \tag{6}$$

where δ is a dimensionless quantity representing the distance, as $\delta = \gamma$, and γ is the magnetic field strength.

The magnitude of $\vec{H} = H$ is

$$\begin{aligned} H(x,r) &= \sqrt{H_x^2 + H_r^2} \\ &= \frac{\gamma}{2\pi} \cdot \frac{x^2}{x^2 + (r+d)^2}, \end{aligned} \tag{7}$$

where the components H_x and H_r are given by

$$\begin{aligned} H_x(x,r) &= -\frac{\partial V}{\partial x} \\ &= \frac{\gamma}{2\pi} \cdot \frac{x^2 - (r+d)^2}{\left(x^2 + (r+d)^2\right)^2}, \\ H_r(x,r) &= -\frac{\partial V}{\partial r} \\ &= \frac{\gamma}{2\pi} \cdot \frac{2x(r+d)}{\left(x^2 + (r+d)^2\right)^2}. \end{aligned} \tag{8}$$

Following references [49–51], we also obtain the gradient of the magnetic field of strength by expanding (7) in powers of x and retaining up to powers x^2, which gives us the following:

$$\begin{cases} \dfrac{\partial H}{\partial x} \approx -\dfrac{\gamma}{\pi} \cdot \dfrac{x}{(r+d)^4}, \\ \dfrac{\partial H}{\partial r} \approx -\dfrac{\gamma}{\pi}\left(-\dfrac{1}{(r+d)^3} + \dfrac{2x^2}{(r+d)^5}\right). \end{cases} \tag{9}$$

Finally, the magnetic field of intensity $H(x,r)$ is given by

$$H(x,r) \approx \frac{\gamma}{2\pi}\left(\frac{1}{(r+d)^2} - \frac{x^2}{(r+d)^4}\right). \tag{10}$$

Previous studies of FHD, such as [51], found that fluid magnetization corresponds to temperature and magnetic field intensity. Moreover, the following relation holds for magnetization:

$$M = K(T_c - T), \tag{11}$$

where the symbols T_c and K represent the Curie temperature and pyromagnetic coefficient, respectively.

In Table 1, ϕ represents the magnetic particles' fraction volume, and d_f and d_p are the diameter of the blood (base fluid) and Fe_3O_4 (magnetic particles), respectively. The magnetic particle shape factor is represented by m. That is, $m = 3$ indicates our shape is spherical, and $m = 6.3698$ indicates we have a cylindrical shape [52]. Additionally, the subscript symbols $_f$ and $_s$ represent the base fluid (blood) and magnetic particles (Fe_3O_4), respectively. For our numerical simulations, we shall assume that the diameter of blood is $d_f = 25\,nm$, and that magnetic particles Fe_3O_4 are in a cylindrical shape ($m = 6.3698$) with a diameter of $d_p = 5\,nm$.

3. Similarity Transformations

To nondimensionalize equations (1) to (3), we introduced the following transformations as performed in references [44, 45]:

$$\begin{cases} \eta = \dfrac{Ur^2}{\nu_f x}, \\ \psi = \nu_f x f(\eta), \\ \theta(\eta) = \dfrac{T_c - T}{T_c - T_w}, \end{cases} \tag{12}$$

where ψ is assumed to be a stream function that satisfies the continuity equation such that the following conditions hold:

$$\begin{aligned} u &= \frac{1}{r}\frac{\partial \psi}{\partial r}, \\ v &= -\frac{1}{r}\frac{\partial \psi}{\partial x}. \end{aligned} \tag{13}$$

Now, using (12) and (13) along with Table 1, and substituting them into equations (2) to (4), gives us the following nonlinear differential equations:

$$\eta f''' + f'' + A_1\frac{f}{2}f'' - A_2\frac{Mn}{4}f' - A_3\frac{\beta\eta^2\theta}{(\eta+\alpha)^4} = 0, \tag{14}$$

$$\eta\theta'' + \theta' - A_4\Pr\frac{f}{2}\theta' + A_5\beta Ec(\varepsilon - \theta)\left[\frac{\eta^2 f'}{(\eta+\alpha)^4} + \frac{\eta^3 f' - \eta^2 f}{(\eta+\alpha)^5}\right] - A_6 Mn\mathrm{Ec}\left(f'\right)^2 = 0. \tag{15}$$

such that

$$\begin{aligned} f(c) &= \frac{\lambda}{2}c, \\ f'(c) &= \frac{\lambda}{2}, \\ \theta(c) &= 1, \\ f'(\infty) &\longrightarrow 0, \\ \theta(\infty) &\longrightarrow 0. \end{aligned} \tag{16}$$

In (14) and (15) above, the parameters $\beta = (\gamma/2\pi)(\mu_0 K(T_c - T_w)\rho_f/\mu_f^2)$ represent the ferromagnetic interaction parameter, $\varepsilon = (T_c/T_c - T_w)$ is the Curie temperature, $\alpha = \sqrt{Ur/\nu_f x d^2}$ is the dimensionless quantity that represents the distance, $\Pr = ((\mu C_p)_f/\kappa_f)$ is the Prandtl number, $Mn = (\sigma_f\mu_0^2 H^2 x/U\rho_f)$ is the magnetic field parameter, $\lambda = (u_w/U)$ is the velocity ratio parameter, and $Ec = (\nu_f U^2/\kappa_f(T_c - T_w))$ is the Eckert number.

Finally, the coefficients A_1, A_2, A_3, A_4, A_5, and A_6 are given by

$$\begin{aligned} A_1 &= \left[1 - 34.87\left(\frac{d_p}{d_f}\right)^{-0.3}\phi^{1.03}\right]\cdot\left[1 - \phi + \phi\frac{\rho_s}{\rho_f}\right], \\ A_2 &= \left[1 - 34.87\left(\frac{d_p}{d_f}\right)^{-0.3}\phi^{1.03}\right]\cdot\left[1 + \frac{3\left(\sigma_s/\sigma_f - 1\right)\phi}{\left(\sigma_s/\sigma_f + 1\right) - \left(\sigma_s/\sigma_f - 1\right)\phi}\right], \\ A_3 &= \left[1 - 34.87\left(\frac{d_p}{d_f}\right)^{-0.3}\phi^{1.03}\right], \\ A_4 &= \frac{\kappa_f}{\kappa_{mf}}\left[1 - \phi + \phi\frac{\left(\rho C_p\right)_s}{\left(\rho C_p\right)_f}\right], \\ A_5 &= \frac{\kappa_f}{\kappa_{mf}}, \\ A_6 &= \frac{\kappa_f}{\kappa_{mf}}\left[1 + \frac{3\left(\sigma_s/\sigma_f - 1\right)\phi}{\left(\sigma_s/\sigma_f + 1\right) - \left(\sigma_s/\sigma_f - 1\right)\phi}\right]\cdot\frac{1}{\left(1 - \phi + \phi\sigma_s/\sigma_f\right)}. \end{aligned} \tag{17}$$

Table 1: The thermophysical properties of magnetic fluid according to their definition as in references [45, 52–54].

Magnetic fluid properties	Applied model
Density	$\rho_{mf} = (1-\phi)\rho_f + \phi\rho_s$
Dynamic viscosity	$(\mu_{mf}/\mu_f) = (1/1 - 34.87(d_p/d_f)^{-0.3}\phi^{1.03})$
Heat capacitance	$(\rho C_p)_{mf} = (1-\phi)(\rho C_p)_f + \phi(\rho C_p)_s$
Electrical conductivity	$(\sigma_{mf}/\sigma_f) = 1 + (3((\sigma_s/\sigma_f) - 1)\phi/((\sigma_s/\sigma_f) + 1) - ((\sigma_s/\sigma_f) - 1)\phi)$
Thermal conductivity	$(\kappa_{mf}/\kappa_f) = ((\kappa_s + (m-1)\kappa_f) - (m-1)\phi(\kappa_f - \kappa_s)/(\kappa_s + (m-1)\kappa_f) + \phi(\kappa_f - \kappa_s))$

4. Physical Quantities

In our work, we are interested in studying how the physical quantities, such as the skin friction coefficient C_f and local Nusselt number Nu, affect our model. The quantities are defined as

$$C_f = \frac{\mu_{mf}}{\rho_f U^2}\left(\frac{\partial u}{\partial r}\right)_{r=R}, \qquad Nu = \frac{x}{(T_c - T_w)}\left(\frac{\partial T}{\partial r}\right)_{r=R}. \tag{18}$$

Now, using (12) and (13), the final results of wall drag force and the rate of heat transfer become

$$C_f = \frac{4}{1 - 34.87\left(d_p/d_f\right)^{-0.3}\phi^{1.03}}\mathrm{Re}^{-(1/2)}c^{(1/2)}f'(c), \qquad Nu = -2\mathrm{Re}^{(1/2)}c^{(1/2)}\theta'(c), \tag{19}$$

where $\mathrm{Re} = (Ux/\nu_f)$ is the local Reynolds number.

5. Numerical Simulations

For our model, a two-point boundary value problem can be formed by coupling the nonlinear ODEs in (14) and (15) along with the boundary conditions in (16). The BVP can be solved numerically by using a technique proposed by Kafoussias et al. [55]. The authors showed that although their numerical approach was fairly simple, it was efficient and yielded accurate results. Their technique was a central spacing finite difference method. Furthermore, a tridiagonal matrix manipulation process was used and solved using an iterative method. Details about the same numerical procedure can be found in [12, 48].

Following [55], we can rewrite the momentum (14) as follows:

$$\eta f''' + \left(1 + A_1\frac{f}{2}\right)f'' - A_2\frac{Mn}{4}f' = A_3\frac{\beta\eta^2\theta}{(\eta+\alpha)^4}. \tag{20}$$

Further simplifying yields

$$\eta(f')'' + \left(1 + A_1\frac{f}{2}\right)(f')' - A_2\frac{Mn}{4}f' = A_3\frac{\beta\eta^2\theta}{(\eta+\alpha)^4}. \tag{21}$$

Now, to reduce the order of the differential equation, we substitute $g = f'$ in (21), which gives us

$$Pg'' + Qg' + Rg = S, \tag{22}$$

where

$$P = \eta, Q, \quad = \left(1 + A_1\frac{f}{2}\right), \quad R = -A_2\frac{Mn}{4}, \quad S = A_3\frac{\beta\eta^2\theta}{(\eta+\alpha)^4}. \tag{23}$$

Similarly, the second-order energy differential (15) can be written as

$$\eta\theta'' + \left(1 - A_4\mathrm{Pr}\frac{f}{2}\right)\theta' - A_5\beta Ec\left[\frac{\eta^2 f'}{(\eta+\alpha)^4} + \frac{\eta^3 f' - \eta^2 f}{(\eta+\alpha)^5}\right]\theta = -A_5\beta Ec\varepsilon\left[\frac{\eta^2 f'}{(\eta+\alpha)^4} + \frac{\eta^3 f' - \eta^2 f}{(\eta+\alpha)^5}\right] + A_6 MnEc\left(f'\right)^2. \tag{24}$$

By further simplifying, (24) becomes

$$Pg'' + Qg' + Rg = S, \tag{25}$$

where $g = \theta, P = \eta, Q = (1 - A_4\mathrm{Pr}f/2), R = -A_5\beta Ec[\eta^2 f'/(\eta+\alpha)^4 + \eta^3 f' - \eta^2 f/(\eta+\alpha)^5]$, $S = -A_5\beta Ec\varepsilon[\eta^2 f'/(\eta+\alpha)^4 + \eta^3 f' - \eta^2 f/(\eta+\alpha)^5] + A_6 MnEc(f')^2$.

We now numerically solve the set of (21) and (24) using the scheme mentioned earlier. We start by providing an initial guess for the values of $f'(\eta)$ and $\theta(\eta)$ that is between $\eta = c$ and $\eta = \eta_\infty (\eta \longrightarrow \infty)$ that satisfies the boundary conditions in (16).

Now, by using the values $\lambda = 1$ and $c = 0.1$, the boundary conditions will be satisfied whenever

$$f(\eta) = 0.06 - \frac{\eta}{\eta_\infty},$$
$$f'(\eta) = 0.51 - \frac{\eta}{\eta_\infty}, \quad (26)$$
$$\theta(\eta) = 1.01 - \frac{\eta}{\eta_\infty}.$$

We can obtain the values of $f(\eta)$ by integrating $f'(\eta)$. This is numerically done by first retaining the values of $\theta(\eta)$ while seeking a newer estimation f'_{new} for $f'(\eta)$ by solving (21). The newer values are then updated for $f(\eta)$ and $f'(\eta)$. This process of solving (21) and consequently (14) is iteratively solved till the desired convergence with a small tolerance value of ε_1 is reached. By using the converged $f(\eta)$ values, we can solve (24) to obtain the values for the temperature distribution $\theta(\eta)$. This numerical scheme is performed until convergence is reached within our ε_1 tolerance.

For our numerical simulations, we used a step size of $h = \Delta\eta = 0.01$ and $0 \le \eta \le 10$. For convergence, our tolerance acceptance level was $\varepsilon_1 = 10^{-3}$.

6. Results and Discussion

We compare the results of our simulations with that of Ishak et al. [56]. For our comparison, the skin friction coefficient was for $\beta = Mn = \phi = \lambda = 0$ with various needle size c values. The comparison is depicted in Table 2, and it clearly shows that our results were fairly accurate as they are within 10^{-2} with that of [56]. Additionally, to estimate the accuracy of our obtained results, we perform an error analysis, and our results are summarized in Table 2. We defined our error percentage to be

$$\text{Error} = \left(\left|\frac{X_p - X_{[56]}}{X_{[56]}}\right|\right) \times 100, \quad (27)$$

where X_p are our numerical results such as $f''(c)$ and $X_{[56]}$ are the numerical results of Ishak et al. in [56]. Furthermore, the physical data for the thermophysical quantities of blood and Fe_3O_4 are represented in Table 3.

The effects of the needle size c on both the velocity $f'(\eta)$ and the temperature $\theta(\eta)$ are presented in Figures 2(a) and 2(b), respectively. The results clearly show that both the axial velocity and temperature profiles increase whenever the values of needle size c are increased. Physically, this may be explained as both the heat and mass diffuse quickly in a needle with a slender surface, compared to that of a needle with a thick surface. Moreover, the highest velocity and blood temperature are attained when the magnetic particles are introduced into the blood compared to regular pure blood.

The effects of the ferromagnetic number β are presented for the axial velocity $f'(\eta)$ and the temperature $\theta(\eta)$ in Figures 3(a) and 3(b), respectively. In Figure 3(a), we see that the velocity decreases whenever the ferromagnetic number β is increased. However, the opposite happens for temperature θ. That is, we see in Figure 3(b) that the temperature θ rises when the ferromagnetic number β is increased, which can be explained as the strong magnetic field can generate a magnetic dipole that is perpendicular to the surface, which initiates a resistive force known as the Kelvin force. This results in the motion of blood having the propensity to slow down, consequently raising the temperature. Additionally, we note that with increasing values of the needle size c, both the fluid velocity and temperature at the boundary layer increase.

Table 2: Comparison of $f''(c)$ values between our simulation and study by Ishak et al. [56] for various needle size c values when $\beta = Mn = \phi = \lambda = 0$, and $Pr = 1$.

c	Present results	Ishak et al. [56]	Error percentage
0.001	62.176	62.1637	0.019786
0.010	8.4910	8.4924	0.016485
0.100	1.2780	1.2888	0.000108

Table 3: The base fluid (blood) and magnetic particles (Fe_3O_4) properties and values are based on references [12, 14, 54].

Physical properties	Blood	Fe_3O_4
$\rho(\text{kgm}^{-3})$	1050	5180
$C_p(\text{jkg}^{-1}\text{K}^{-1})$	3900	670
$\sigma(\text{sm}^{-1})$	0.8	0.74×10^6
$\kappa(\text{Wm}^{-1}\text{K}^{-1})$	0.5	9.7

Figures 4(a) and 4(b) show how the magnetic particle's volume ϕ affects the dimensionless velocity f' and the temperature θ. Our results show that both the velocity $f'(\eta)$ and the temperature $\theta(\eta)$ increase whenever the volume of the magnet particles ϕ increases. This is due to the thermal conductivity of magnetic fluid increasing when more magnetic particles are in the blood, which in turn enhances heat transfer. Furthermore, the thermal boundary layer thickness is also increased as the high concentration of magnetic particles yields a higher ratio of thermal conductivity.

The effects of both the magnetic field parameter Mn and the Eckert number Ec on the dimensionless velocity $f'(\eta)$ are visualized in Figures 5(a) and 5(b), respectively. The Lorentz force's impact on momentum is caused by the application of the magnetic field, and it influences the flow's velocity and direction in the vicinity of the wall. The gradient of this shift will be steeper close to the wall the greater the field value, which affects and amplifies the pressure decrease. When the flow rate is decreased, the fluid inside the wall has more time to transfer heat, the average fluid temperature rises, and heat transfer eventually occurs. This behavior can be seen in Figure 5(a). We also note that when the Eckert number Ec increases, this causes the fluid velocity to decrease. This is because the heat energy is stored in the blood due to frictional heating. As a result, the momentum boundary layer decreases, consequently increasing the thermal boundary layer.

Figures 6(a) and 6(b) visualize how the ferromagnetic number β affects the skin friction coefficient $f''(c)$ and the rate of heat transfer θ' for different magnetic particles' volume fraction ϕ. From Figure 6, it is clearly evident that both the skin friction coefficient $f''(c)$ and the heat transfer

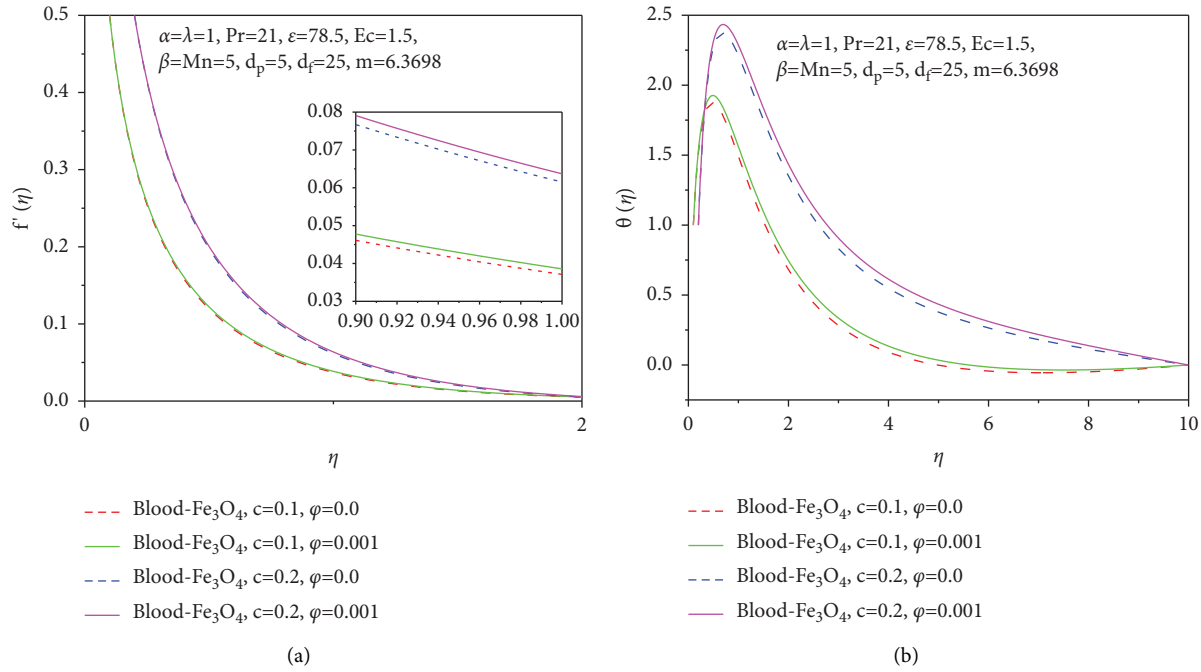

Figure 2: The effects of the needle size c on the velocity (a) and on the temperature θ (b).

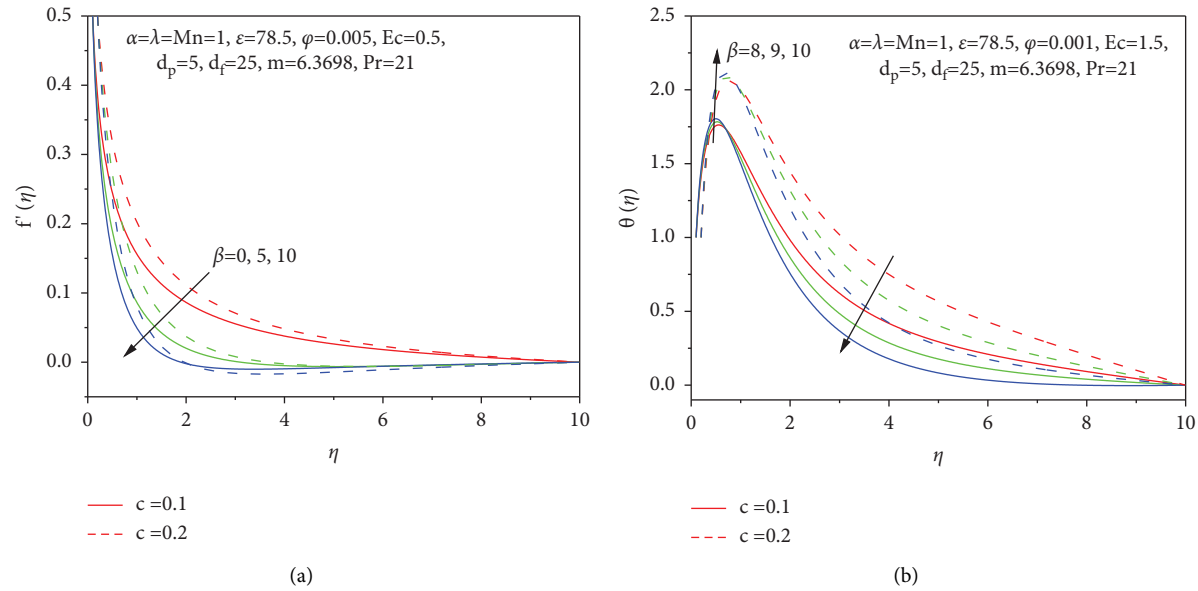

Figure 3: The effects of the ferromagnetic number β on the velocity (a) and the temperature (b).

rate $-\theta'(c)$ increase whenever the ferromagnetic number β increases. The major decrement of $f''(c)$ is found for a slender needle-sized surface while for a relatively thicker needle, the rate of heat transfer increases appreciably.

Figures 7(a) and 7(b) visualize how the magnetic particles' volume ϕ affects the skin friction coefficient $f''(c)$ and the heat transfer rate $-\theta'(c)$, respectively. It is apparent from the aforementioned figures that the volume fraction $f''(c)$ increases, whereas the heat transfer rate $-\theta'(c)$ decreases when the magnetic particles' volume ϕ increases.

Finally, the effects of the magnetic field parameter Mn on both the skin friction coefficient $f''(c)$ and the heat transfer rate $-\theta'(c)$ are visualized in Figures 8(a) and 8(b), respectively. From Figure 8(a), we clearly see that as Mn increases, then the resulting skin friction coefficient $f''(c)$ decreases. However, in Figure 8(b), we see that the heat transfer rate increases whenever the magnetic field parameter Mn is increased.

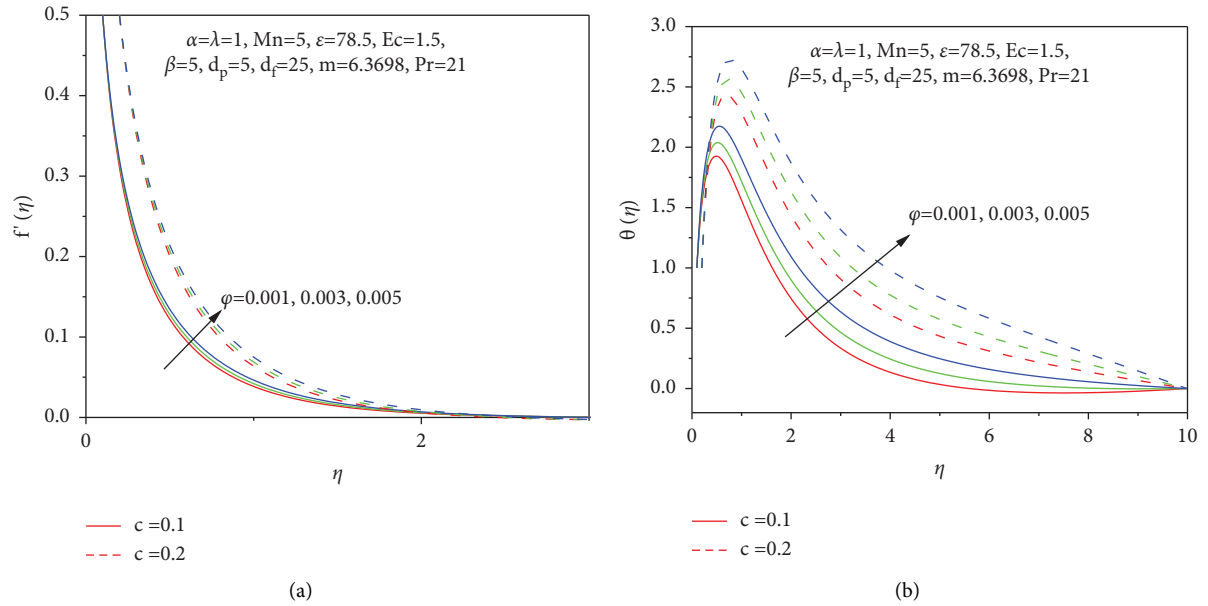

Figure 4: The effect of the magnetic particle's volume ϕ on the velocity (a) and the temperature (b).

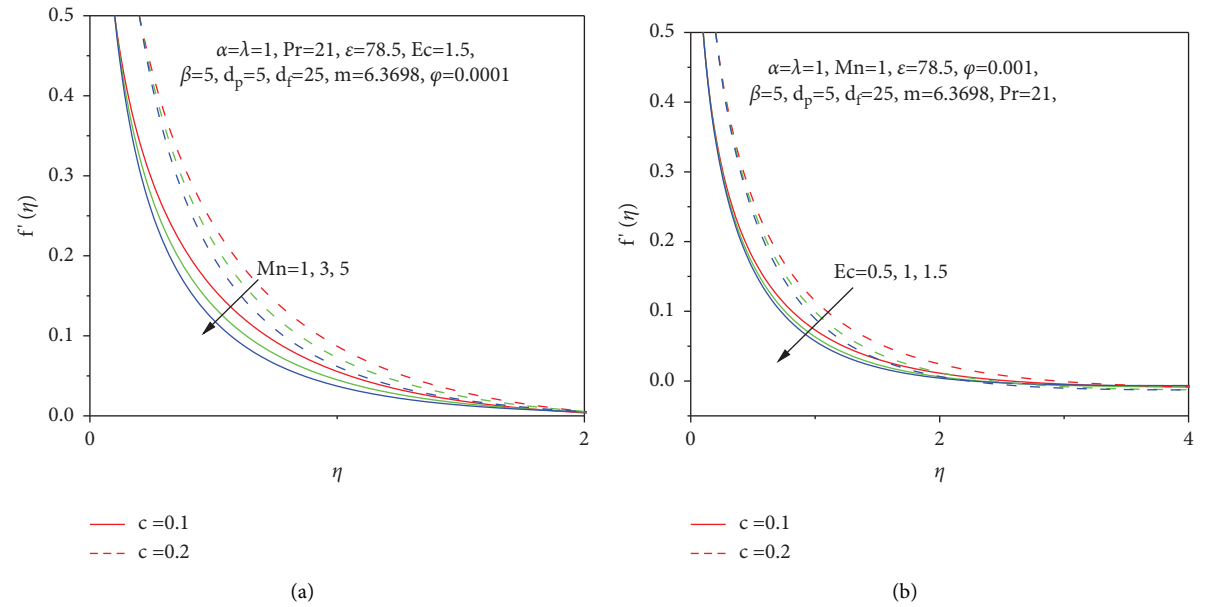

Figure 5: (a): The effects of the magnetic field parameter *Mn* on the velocity. (b): The effects of the Eckert number *Ec* on the velocity.

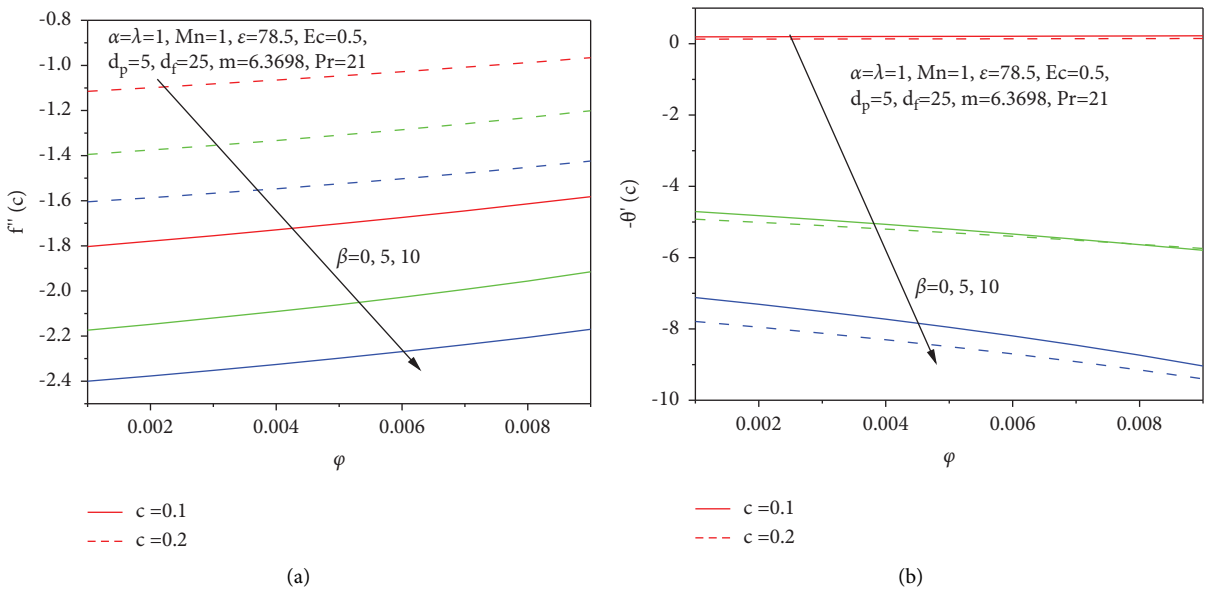

Figure 6: (a): The effects of the ferromagnetic number β on the skin friction coefficient $f''(c)$. (b): The effects of the ferromagnetic number β on the heat transfer rate $-\theta'(c)$.

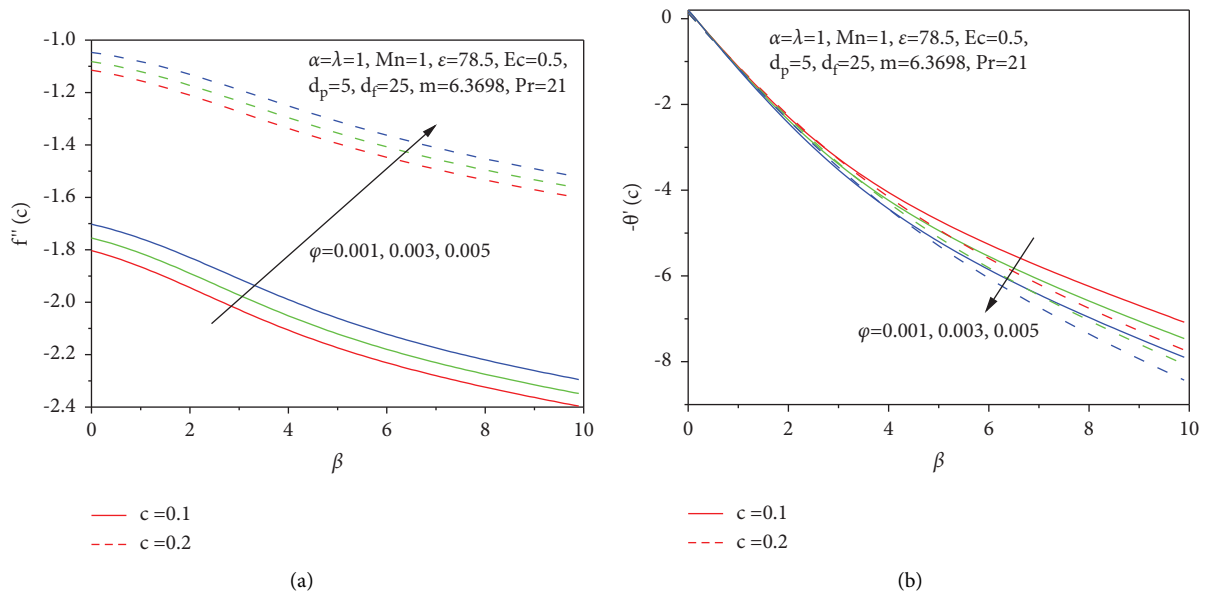

Figure 7: (a): The effects of the magnetic particle's volume ϕ on the skin friction. (b): The effects of the magnetic particle's volume ϕ on the heat transfer rate.

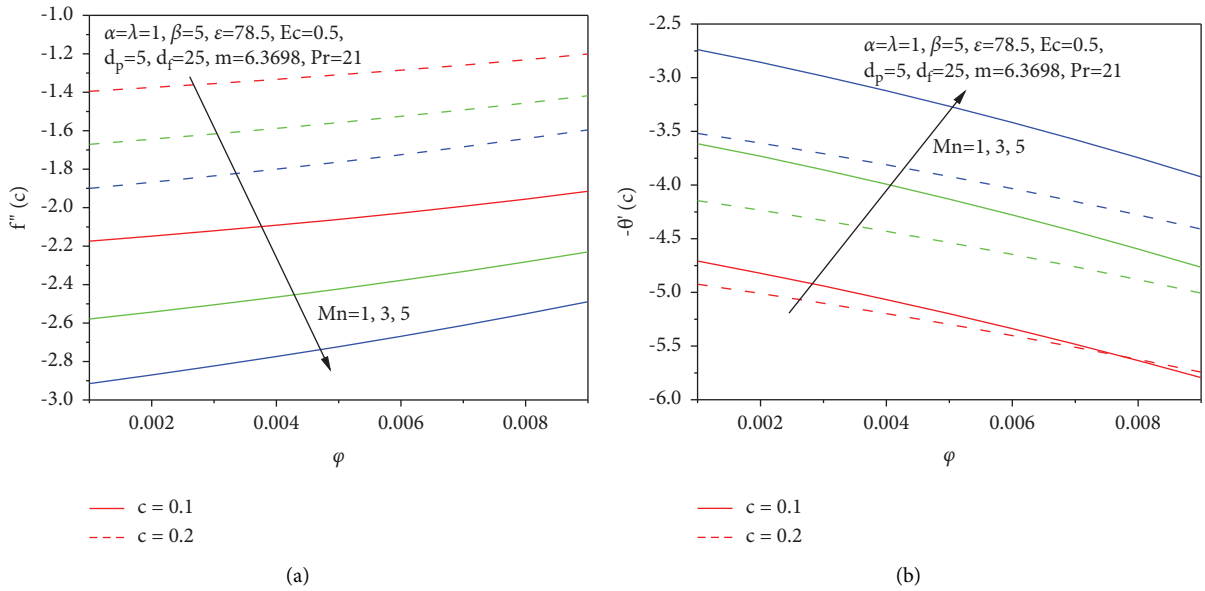

FIGURE 8: (a): The effects of the magnetic field parameter Mn on the skin friction coefficient. (b): The effects of the magnetic field parameter Mn on heat transfer rate.

7. Conclusions

In this paper, a two-dimensional, steady, laminar flow, and heat transfer of biomagnetic fluid with magnetic particles is mathematically developed with the aid of magnetohydrodynamics and ferrohydrodynamics along a thin needle. Our most prominent results obtained from the simulations are summarized as follows, and we found that

(i) The axial fluid velocity, temperature profiles, local Nusselt number, and drag force coefficient rise when the values of the needle size are increased

(ii) As the ferromagnetic number, magnetic field parameter, and Eckert number increase, the resulting fluid velocity will decrease

(iii) Both the velocity and the temperature increase whenever the magnetic particles' volume fraction increases

(iv) An increase in the ferromagnetic number will lead to a reduction in the skin friction coefficient and the rate of heat transfer

(v) For the magnetic particles volume fraction, the skin friction coefficient increases while the opposite behavior is found in the heat transfer rate

(vi) Increasing the magnetic field parameter leads to the skin friction coefficient decreasing and, at the same time, increases the transfer rate

The obtained results indicate that using magnetic particles in the blood leads to significant control over the flow in the boundary layer regime. Furthermore, the ferromagnetic number plays an essential role in controlling the flow and heat transfer.

Our model closely relates to that of transdermal delivery and electromagnetic treatments. Moreover, these techniques involve a variety of physical factors such as electromagnetic, nanosized scale, hydrodynamic slip, and thermal slip. Therefore, a reliable analysis should include each of these elements.

Biomagnetic nano needle thermal therapy is widely used in clinical applications, especially in treating tumors, and this is performed by the successful implication of pulse electrochemotherapy and DC electrotherapy. For pulse applications, which have an electrical field strength of around 2 kV/cm, needle electrodes must be introduced into the tumor site. Caliper electrodes are only applied directly to the skin for treating skin cancer. A unique noninvasive cancerostatic possibility is provided by external electromagnetic fields (magnetic field strength >5 mT) that are produced by Helmholtz coils or solenoids. However, in the following decades, the transdermal treatments using this adjuvant noninvasive therapy in conjunction with cancer-preventing medicines, hyperthermia, and photodynamic therapy might hold many potentials.

One future extension of our work is to examine the various characteristics of a 2D/3D biomagnetic fluid flow containing magnetic/nonmagnetic particles with velocity, thermal slip, thermal radiation, and heat source/sink features numerically.

Nomenclature

(x, r): Cartesian coordinate system (m)
c: Needle size
(u, v): Components of velocity (m/s)
d: Distance between the magnetic dipole and sheet (m)
C_p: Specific heat at constant pressure ($Jkg^{-1}K^{-1}$)

ρ: Fluid density (kg/m^3)
γ: Strength of magnetic field at the source position
μ: Dynamic viscosity (kg/ms)
μ_0: Magnetic fluid permeability (NA^{-2})
κ: Thermal conductivity (J/msK)
σ: Electrical conductivity
K: Pyromagnetic coefficient (K^{-1})
T_c: Curie temperature (K)
T_w: Temperature of the needle surface (K)
u_w: Needle velocity (m/s)
u_∞: Velocity of the ambient fluid (m/s)
H: Magnetic field strength (A/m)
α: Dimensionless distance
M: Magnetization
Mn: Magnetic field parameter
β: Ferromagnetic interaction parameter
λ: Flow parameter
Pr: Prandtl number
Ec: Eckert number
ϕ: Volume fraction of magnetic particle
ε: Dimensionless Curie temperature
η: Nondimensional space variable
θ: Dimensionless temperature
ψ: Dimensionless stream function
m: Magnetic particle's shape factor
$_f$: For base fluid
$_s$: For magnetic particles.

Data Availability

The data used to support the findings of this study are available from the corresponding author upon request.

Conflicts of Interest

The authors declare that there are no conflicts of interest in this paper.

Acknowledgments

This work was supported and funded by the Kuwait University Research (Grant no. SM05/21).

References

[1] E. K. Ruuge and A. N. Rusetski, "Magnetic fluids as drug carriers: targeted transport of drugs by a magnetic field," *Journal of Magnetism and Magnetic Materials*, vol. 122, no. 1-3, pp. 335–339, 1993.

[2] J. Plavins and M. Lauva, "Study of colloidal magnetite-binding erythrocytes: prospects for cell preparation," *Journal of Magnetism and Magnetic Materials*, vol. 122, no. 1-3, pp. 349–353, 1993.

[3] S. Rashidi, J. A. Esfahani, and M. Maskaniyan, "Applications of magnetohydrodynamics in biological systems-a review on the numerical studies," *Journal of Magnetism and Magnetic Materials*, vol. 439, pp. 358–372, 2017.

[4] J. Liu, G. A. Flores, and R. Sheng, "In-vitro investigation of blood embolization in cancer treatment using magneto-rheological fluids," *Journal of Magnetism and Magnetic Materials*, vol. 225, no. 1-2, pp. 209–217, 2001.

[5] N. K. Prasad, K. Rathinasamy, D. Panda, and D. Bahadur, "Mechanism of cell death induced by magnetic hyperthermia with nanoparticles of γ-$Mn_xFe_{2-x}O_3$ synthesized by a single step process," *Journal of Materials Chemistry*, vol. 17, no. 48, pp. 5042–5051, 2007.

[6] D. D. Stark, R. Weissleder, G. Elizondo et al., "Superparamagnetic iron oxide: clinical application as a contrast for MR imaging," *Radiology*, vol. 168, no. 2, pp. 297–301, 1988.

[7] S. U. Choi and J. A. Eastman, "Enhancing thermal conductivity of fluids with nanoparticles," *American Society Of Mechanical Engineers Fluids Engineering Division*, vol. 66, pp. 99–105, 1995.

[8] S. Nadeem, R. Mehmood, and N. S. Akbar, "Non-orthogonal stagnation point flow of a nano non-Newtonian fluid towards a stretching surface with heat transfer," *International Journal of Heat and Mass Transfer*, vol. 57, no. 2, pp. 679–689, 2013.

[9] M. K. Nayak, "MHD 3D flow and heat transfer analysis of nanofluid by shrinking surface inspired by thermal radiation and viscous dissipation," *International Journal of Mechanical Sciences*, vol. 124-125, pp. 185–193, 2017.

[10] W. Khan and I. Pop, "Boundary-layer flow of a Nanofluid past a stretching sheet," *International Journal of Heat and Mass Transfer*, vol. 53, no. 11-12, pp. 2477–2483, 2010.

[11] F. Ali, S. Majeed, and A. Imtiaz, "Magnetohydrodynamic Blood flow in a cylindrical tube with magnetic particles: a time fractional model," *Mathematical Problems in Engineering*, vol. 2021, Article ID 6624912, 14 pages, 2021.

[12] J. Alam, M. G. Murtaza, E. E. Tzirtzilakis, and M. Ferdows, "Application of biomagnetic fluid dynamics modeling for simulation of flow with magnetic particles and variable fluid properties over a stretching cylinder," *Mathematics and Computers in Simulation*, vol. 199, pp. 438–462, 2022.

[13] M. Ferdows, M. G. Murtaza, E. E. Tzirtzilakis, and F. Alzahrani, "Numerical study of blood flow and heat transfer through stretching cylinder in the presence of a magnetic dipole," *Zeitschrift für Angewandte Mathematik und Mechanik*, vol. 100, no. 7, Article ID e201900278, 2020.

[14] J. Alam, M. G. Murtaza, E. E. Tzirtzilakis, and M. Ferdows, "MagnetoHydrodynamic and FerroHydrodynamic interactions on the biomagnetic flow and heat transfer containing magnetic particles along a stretched cylinder," *European Journal of Computational Mechanics*, vol. 31, no. 1, pp. 1–40, 2022.

[15] S. Sharma, U. Singh, and V. K. Katiyar, "Magnetic field effect on flow parameters of blood along with magnetic particles in a cylindrical tube," *Journal of Magnetism and Magnetic Materials*, vol. 377, pp. 395–401, 2015.

[16] F. Ali, A. Imtiaz, I. Khan, and N. A. Sheikh, "Flow of magnetic particles in blood with isothermal heating: a fractional model for two-phase flow," *Journal of Magnetism and Magnetic Materials*, vol. 456, pp. 413–422, 2018.

[17] T. Hayat, M. I. Khan, M. Farooq, T. Yasmeen, and A. Alsaedi, "Water-carbon nanofluid flow with variable heat flux by a thin needle," *Journal of Molecular Liquids*, vol. 224, pp. 786–791, 2016.

[18] S. N. A. Salleh, N. Bachok, N. M. Arifin, F. M. Ali, and I. Pop, "Magnetohydrodynamics flow past a moving vertical thin needle in a nanofluid with stability analysis," *Energies*, vol. 11, no. 12, p. 3297, 2018.

[19] M. Waleed Ahmed Khan, M. Ijaz Khan, T. Hayat, and A. Alsaedi, "Entropy generation minimization (EGM) of nanofluid flow by a thin moving needle with nonlinear thermal radiation," *Physica B: Condensed Matter*, vol. 534, pp. 113–119, 2018.

[20] N. A. L. Aladdin, N. Bachok, and I. Pop, "Boundary layer flow and heat transfer of Cu-Al2o3/water over a moving horizontal slender needle in presence of hydromagnetic and slip effects," *International Communications in Heat and Mass Transfer*, vol. 123, Article ID 105213, 2021.

[21] M. K. Nayak, R. Mehmood, S. Mishra, A. Misra, and T. Muhammad, "Thermal and velocity slip effects in mixed convection flow of magnetized ceramic nanofluids over a thin needle with variable physical properties," *Waves in Random and Complex Media*, pp. 1–19, 2021.

[22] K. Ganesh Kumar, "Impact of magnetic dipole on flow and heat transfer of AA7072-AA7075/water based nanofluid over a stretching sheet using Koo and Kleinstreuer model," *The European Physical Journal Plus*, vol. 137, no. 6, pp. 669–713, 2022.

[23] M. G. Reddy, K. Ganesh Kumar, and S. A. Shehzad, "A static and dynamic approach of aluminum alloys (AA7072-AA7075) over a semi-infinite heated plate," *Physica Scripta*, vol. 95, no. 12, Article ID 125201, 2020.

[24] K. G. Kumar, E. H. B. Hani, M. E. H. Assad, M. Rahimi-Gorji, S. Nadeem, and S. Nadeem, "A novel approach for investigation of heat transfer enhancement with ferromagnetic hybrid nanofluid by considering solar radiation," *Microsystem Technologies*, vol. 27, no. 1, pp. 97–104, 2021.

[25] B. Souayeh, K. G. Kumar, M. G. Reddy et al., "Slip flow and radiative heat transfer behavior of Titanium alloy and ferromagnetic nanoparticles along with suspension of dusty fluid," *Journal of Molecular Liquids*, vol. 290, Article ID 111223, 2019.

[26] S. A. Shehzad, M. Gnaneswara Reddy, S. A. Shehzad, and F. M. Abbasi, "A least square study on flow and radiative heat transfer of hybrid nanofluid over a moving frame by considering a spherical shape particle," *Revista Mexicana de Física*, vol. 66, no. 2, pp. 162–170, 2020.

[27] M. G. Reddy, M. V. V. N. L. Sudharani, K. G. Kumar, and K. Ganesh Kumar, "An analysis of dusty slip flow through a single-/multi-wall carbon nanotube," *Continuum Mechanics and Thermodynamics*, vol. 32, no. 3, pp. 971–985, 2020.

[28] M. Gnaneswara Reddy, M. Sudha Rani, K. Ganesh Kumar, B. Prasannakumar, H. Lokesh, and H. J. Lokesh, "Hybrid dusty fluid flow through a Cattaneo–Christov heat flux model," *Physica A: Statistical Mechanics and Its Applications*, vol. 551, Article ID 123975, 2020.

[29] M. G. Reddy and K. G Kumar, "Cattaneo-Christov heat flux feature on carbon nanotubes filled with micropolar liquid over a melting surface: a stream line study," *International Communications in Heat and Mass Transfer*, vol. 122, Article ID 105142, 2021.

[30] S. Das, P. Karmakar, and A. Ali, "Electrothermal blood streaming conveying hybridized nanoparticles in a non-uniform endoscopic conduit," *Medical, & Biological Engineering & Computing*, vol. 60, no. 11, pp. 3125–3151, 2022.

[31] S. Das, T. K. Pal, R. N. Jana, and B. Giri, "Ascendancy of electromagnetic force and Hall currents on blood flow carrying Cu-Au NPs in a non-uniform endoscopic annulus having wall slip," *Microvascular Research*, vol. 138, Article ID 104191, 2021.

[32] S. Das, T. K. Pal, R. N. Jana, and B. Giri, "Significance of Hall currents on hybrid nano-blood flow through an inclined artery having mild stenosis: homotopy perturbation approach," *Microvascular Research*, vol. 137, Article ID 104192, 2021.

[33] S. Das, T. K. Pal, and R. N. Jana, "Electromagnetic hybrid nano-blood pumping via peristalsis through an endoscope having blood clotting in presence of Hall and ion slip currents," *BioNanoScience*, vol. 11, no. 3, pp. 848–870, 2021.

[34] S. Das, B. Barman, R. N. Jana, and O. D. Makinde, "Hall and ion slip currents' impact on electromagnetic blood flow conveying hybrid nanoparticles through an endoscope with peristaltic waves," *BioNanoScience*, vol. 11, no. 3, pp. 770–792, 2021.

[35] A. Ali, R. N. Jana, and S. Das, "Significance of entropy generation and heat source: the case of peristaltic blood flow through a ciliated tube conveying Cu-Ag nanoparticles using Phan-Thien-Tanner model," *Biomechanics and Modeling in Mechanobiology*, vol. 20, no. 6, pp. 2393–2412, 2021.

[36] F. A. Alwawi, H. T. Alkasasbeh, A. M. Rashad, and R. Idris, "MHD natural convection of Sodium Alginate Casson nanofluid over a solid sphere," *Results in Physics*, vol. 16, Article ID 102818, 2020.

[37] M. Z. Swalmeh, H. T. Alkasasbeh, A. Hussanan, and M. Mamat, "Heat transfer flow of Cu-water and Al_2O_3-water micropolar nanofluids about a solid sphere in the presence of natural convection using Keller-box method," *Results in Physics*, vol. 9, pp. 717–724, 2018.

[38] F. A. Alwawi, A. S. Hamarsheh, H. T. Alkasasbeh, and R. Idris, "Mixed convection flow of magnetized Casson nanofluid over a cylindrical surface," *Coatings*, vol. 12, no. 3, p. 296, 2022.

[39] A. S. Hamarsheh, F. A. Alwawi, H. T. Alkasasbeh, A. M. Rashad, and R. Idris, "Heat transfer improvement in MHD natural convection flow of graphite oxide/carbon nanotubes-methanol based Casson nanofluids past a horizontal circular cylinder," *Processes*, vol. 8, no. 11, p. 1444, 2020.

[40] B. Thomas and K. M. Sumam, "Blood flow in human arterial system-A review," *Procedia Technology*, vol. 24, pp. 339–346, 2016.

[41] D. N. Ku, "Blood flow in arteries," *Annual Review of Fluid Mechanics*, vol. 29, no. 1, pp. 399–434, 1997.

[42] F. Yilmaz and M. Y. Gundogdu, "A critical review on blood flow in large arteries; relevance to blood rheology, viscosity models, and physiologic conditions," *Korea-Australia Rheology Journal*, vol. 20, no. 4, pp. 197–211, 2008.

[43] M. Ramzan, N. S. Khan, and P. Kumam, "Mechanical analysis of non-Newtonian nanofluid past a thin needle with dipole effect and entropic characteristics," *Scientific Reports*, vol. 11, no. 1, Article ID 19378, 2021.

[44] P. Prashar, O. Ojjela, P. K. Kambhatla, and S. K. Das, "Numerical investigation of boundary layer flow past a thin heated needle immersed in hybrid nanofluid," *Indian Journal of Physics*, vol. 96, no. 1, pp. 137–150, 2022.

[45] M. K. Nayak, S. D. Oloniiju, S. Mondal, S. P. Goqo, and P. Sibanda, "Flow and heat transfer over a thin needle immersed in a porous medium filled with an Al_2O_3-water nanofluids using Buongiorno's two-phase model," *International Journal of Ambient Energy*, vol. 43, pp. 3652–3660, 2020.

[46] O. Anwar Beg, F. T. Zohra, M. J. Uddin, A. I. M. Ismail, and S. Sathasivam, "Energy conservation of nanofluids from a biomagnetic needle in the presence of Stefan blowing: lie symmetry and numerical simulation," *Case Studies in Thermal Engineering*, vol. 24, Article ID 100861, 2021.

[47] S. Das, S. Chakraborty, R. N. Jana, and O. D. Makinde, "Entropy analysis of unsteady magneto-nanofluid flow past accelerating stretching sheet with convective boundary condition," *Applied Mathematics and Mechanics*, vol. 36, no. 12, pp. 1593–1610, 2015.

[48] M. G. Murtaza, E. E. Tzirtzilakis, and M. Ferdows, "Effect of electrical conductivity and magnetization on the biomagnetic fluid flow over a stretching sheet," *Zeitschrift fur angewandte Mathematik und Physik (ZAMP)*, vol. 68, no. 4, p. 93, 2017.

[49] N. G. Kafoussias and E. E. Tzirtzilakis, "Biomagnetic fluid flow over a stretching sheet with nonlinear temperature dependent magnetization," *Zeitschrift for Angewandte Mathematik und Physik (ZAMP)*, vol. 54, no. 4, pp. 551–565, 2003.

[50] E. E. Tzirtzilakis and G. B. Tanoudis, "Numerical study of biomagnetic fluid flow over a stretching sheet with heat transfer," *International Journal of Numerical Methods for Heat and Fluid Flow*, vol. 13, no. 7, pp. 830–848, 2003.

[51] H. I. Andersson and O. A. Valnes, "Flow of a heated ferrofluid over a stretching sheet in the presence of a magnetic dipole," *Acta Mechanica*, vol. 128, no. 1-2, pp. 39–47, 1998.

[52] R. Kandasamy, N. A. Bt Adnan, and R. Mohammad, "Nanoparticles shape effects on squeezed MHD flow of water based on Cu, Al_2O_3 and SWCNTs over a porous sensor surface," *Alexandria Engineering Journal*, vol. 57, no. 3, pp. 1433–1445, 2018.

[53] O. D. Makinde, "Stagnation point flow with heat transfer and temporal stability of ferrofluid past a permeable stretching/shrinking sheet," *Defect and Diffusion Forum*, vol. 387, pp. 510–522, 2018.

[54] J. Alam, G. Murtaza, E. Tzirtzilakis, and M. Ferdows, "Biomagnetic fluid flow and heat transfer study of Blood with Gold nanoparticles over a stretching sheet in the presence of Magnetic dipole," *Fluid*, vol. 6, no. 3, p. 113, 2021.

[55] N. G. Kafoussias and E. W. Williams, "An improved approximation technique to obtain numerical solution of a class of two point boundary value similarity problems in fluid mechanics," *International Journal for Numerical Methods in Fluids*, vol. 17, no. 2, pp. 145–162, 1993.

[56] A. Ishak, R. Nazar, and I. Pop, "Boundary layer flow over a continuously moving thin needle in a parallel free stream," *Chinese Physics Letters*, vol. 24, no. 10, pp. 2895–2897, 2007.